

REGULAR PAPER

Time-resolved curling-probe measurements of electron density in high frequency pulsed DC discharges

To cite this article: Anil Pandey *et al* 2016 *Jpn. J. Appl. Phys.* **55** 016101

View the [article online](#) for updates and enhancements.

You may also like

- [Mineralogical Criteria for the Parent Asteroid of the "Carbonaceous" Achondrite NWA 6704](#)
Allison M. McGraw, Vishnu Reddy, Matthew R. M. Izawa et al.
- [Porous Core/Shell Ni@NiO/Pt Hybrid Nanowire Arrays as a High Efficient Electrocatalyst for Alkaline Direct Ethanol Fuel Cells](#)
Maksudul Hasan, Simon B. Newcomb and Kafil M. Razeeb
- [Presolar Silicate and Oxide Grains Found in Lithic Clasts from Isheyevo and the Fine-grained Matrix of Northwest Africa 801](#)
Manish N. Sanghani, Kuljeet Kaur Marhas, Silver Sung-Yun Hsiao et al.



Time-resolved curling-probe measurements of electron density in high frequency pulsed DC discharges

Anil Pandey^{1*}, Wataru Sakakibara², Hiroyuki Matsuoka², Keiji Nakamura¹, and Hideo Sugai^{1*}

¹Department of Engineering, Chubu University, Kasugai, Aichi 487-8501, Japan

²DOWA Thermotech Co., Ltd., Nagoya 467-0854, Japan

*E-mail: anilpandey.only@gmail.com; sugai-h@isc.chubu.ac.jp

Received August 31, 2015; revised October 15, 2015; accepted November 9, 2015; published online December 18, 2015

A plasma-induced shift in the resonance frequency of a curling probe measured by using a network analyzer (NWA) yields the electron density. This technique was applied here for measuring time-varying electron density in pulsed DC glow discharges. Using the NWA in an *on-sweep* synchronization mode with the discharge pulse allows measuring at pulse frequencies below 0.5 kHz. For higher pulse frequencies, an *on-point* mode was introduced which enabled time-resolved measurements of electron density at pulse frequencies reaching 25 kHz, with the minimal time interval of 2 μ s, typically for nitrogen discharge at 10 Pa. In the afterglow regime, the decay time constant of electron density was measured for nitrogen and argon discharges at 40 Pa. In the case of argon, the electron density was observed to decrease in three steps. This characteristic behavior was tentatively attributed to a bi-Maxwellian electron energy distribution and Ramsauer effect, supported by Langmuir probe measurements. © 2016 The Japan Society of Applied Physics

1. Introduction

Among the different types of plasma diagnostic tools, the Langmuir probe technique¹⁾ enables local estimation of plasma parameters such as electron density, electron temperature, and plasma potential. This technique is among the most commonly used ones; however, deposition of insulating thin films when operated in reactive plasmas significantly affects its performance. Moreover, the probe electrode may induce metal contamination, which should be avoided in semiconductor processing. Plasma oscillation method²⁾ enables accurate measurements of electron density based on observations of electron plasma oscillations excited by the beam instability. However, this method also suffers from metal impurities that are released within a relatively short lifetime of a tungsten filament that is used in this method. Plasma absorption probe (also referred to as a surface wave probe) can be used for measuring the plasma electron density³⁻⁵⁾ and electron temperature⁶⁻¹²⁾ without metal contaminations, even in the situation wherein the plasma deposits a non-conducting layer on the probe. However, this technique exhibits weak measurement accuracy for high pressure (>100 Pa) and low electron density (< 5 $\times 10^9$ cm⁻³) plasmas.

On the other hand, a microwave resonator probe^{13,14)} (also referred to as a hairpin probe) is available for the local electron density measurements. This probe utilizes a dipole resonance along its U-shaped wire antenna: the resonance frequency increases with increasing electron density. However, metal impurities are created when this probe is inserted into plasma, and a long antenna arm can disturb the measurements. To overcome these drawbacks, a planar slot-type microwave resonator probe, also called the *curling probe* (CP), has been developed,¹⁵⁾ in which the antenna surface is covered by a thin dielectric plate. Owing to the 1/4-wavelength resonance, the CP resonates at the frequency f_0 (GHz) in vacuum, before a discharge. After the discharge, the resonance frequency increases to f (GHz) in plasma, depending on the electron density n_e (cm⁻³). Based on the measured two resonance frequencies, the electron density is computed from the following simple equation:

$$n_e = \gamma \frac{f^2 - f_0^2}{0.806} \times 10^{10}. \quad (1)$$

Here, the coefficient γ depends on the antenna length, the dielectric cover plate, and the probe geometry.^{16,17)} In the case of a 100-mm-long antenna and a 0.2-mm-thick quartz cover, the value of $\gamma = 5.1$ was obtained. The simplified analytical theory¹⁶⁾ that was used for deriving Eq. (1) is valid for low pressure (<200 Pa).

CP is a compact robust monitoring tool with a minimal diameter of ~6 mm, and is commercially available.¹⁸⁾ In addition, an opto-curling probe (OCP)¹⁹⁻²¹⁾ has been developed that enables simultaneous measurements of electron density and optical emissions. CP and OCP do not suffer from the metal contamination problem, owing to its aluminum or yttrium coating, and can withstand high temperatures of ~600 °C.

Apart from constant-power stationary plasmas, time-modulated pulsed plasmas are also frequently used for plasma processing of materials. Pulsed plasmas have been reported to exhibit improved etching and deposition rates,²²⁾ reduced formation of dust particles,²³⁻²⁶⁾ and uniformity of deposition.^{22,27,28)} However, techniques for time-resolved measurements of electron density are largely lacking, particularly for deposition processes in which diagnostics tools are also deposited. Recently, a CP has been applied to pulsed DC discharges in nitrogen, using the *on-sweep* network analyzer (NWA) mode.²⁹⁾ In pulsed plasma, the resonance frequency varies with time owing to the temporal variation in the electron density. It was demonstrated that temporal density variations can be measured if the synchronization condition is satisfied. However, in these experiments the temporal resolution was poor and the measurement was restricted to slow pulse discharges with large duty cycle ratios.

To overcome this limitation, an *on-point* mode was introduced in the present work. As a result, the temporal resolution was improved and temporal variations in the electron density were successfully measured by using the CP-based technique for discharges with pulse frequencies reaching 25 kHz. The electron density decay in the afterglow

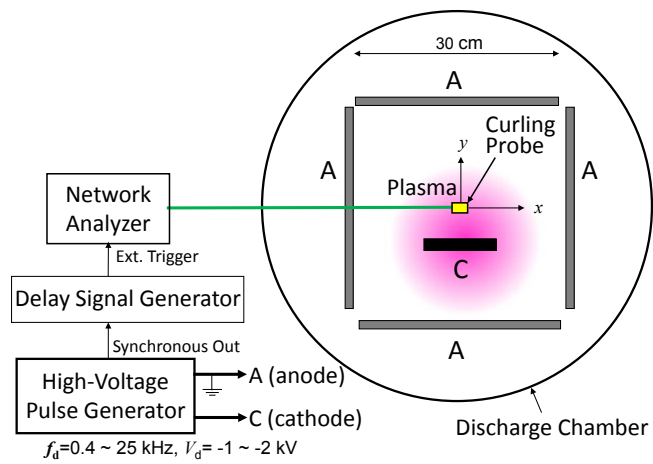


Fig. 1. (Color online) Experimental setup for pulsed plasma production with CP diagnostics.

regime was measured in nitrogen and argon, and a three-step decay for the argon discharge is discussed.

2. Experimental methods

The experiment was conducted in a 60-cm-diameter and 50-cm-long DC glow discharge device that is shown in Fig. 1. This device was specifically designed for metal nitridation, so that a pulsed plasma is mainly produced in the nitrogen gas, although other gases such as argon, hydrogen, and methane are also available. A negative high voltage (−1 to −2 kV) was applied, typically at 10 Pa nitrogen, at the pulse repetition frequency of f_d ($= 0.4\text{--}25$ kHz), to the cathode C (diameter, 13 cm), with five sets of grounded anodes A ($30 \times 30\text{ cm}^2$). The duty cycle ratio (DR = discharge ON time/discharge pulse period) could be varied in a wide range of 10–50%. The 1.6-cm-diameter CP was positioned at the center ($x = y = z = 0$) of the chamber, 5 cm above the cathode ($y = -5$ cm). The grounded anode centers were located at $x = -15$ cm, $x = 15$ cm, $y = 15$ cm, $y = -17$ cm, and $z = -15$ cm.

Calibration of a cable connecting the NWA and the CP head was always performed for canceling spurious signals that were caused by the reflection at the connector and cable loss. The CP was coated with alumina (Al_2O_3), making the probe electrically insulated and resistant to corrosion and arc ignition that can occur during discharge. A synchronous output from a high-voltage pulse source was connected to an external trigger port of the NWA. In the present study, we used the NWA of Agilent E5071C, with two measurement modes (*on-sweep* mode, *on-point* mode), as described in the next section.

3. Reflectance measurements by using the *on-sweep* and *on-point* modes

3.1 *On-sweep* mode

Electron density is derived from the CP resonance frequency according to Eq. (1), while the resonance frequency is determined from a reflectance spectrum obtained by sweeping the NWA frequency. In the case of pulse-modulated plasma, the electron density changes in time, yielding temporal variations in the reflectance spectrum and resonance frequency during the frequency sweeping. To measure the frequency spectrum

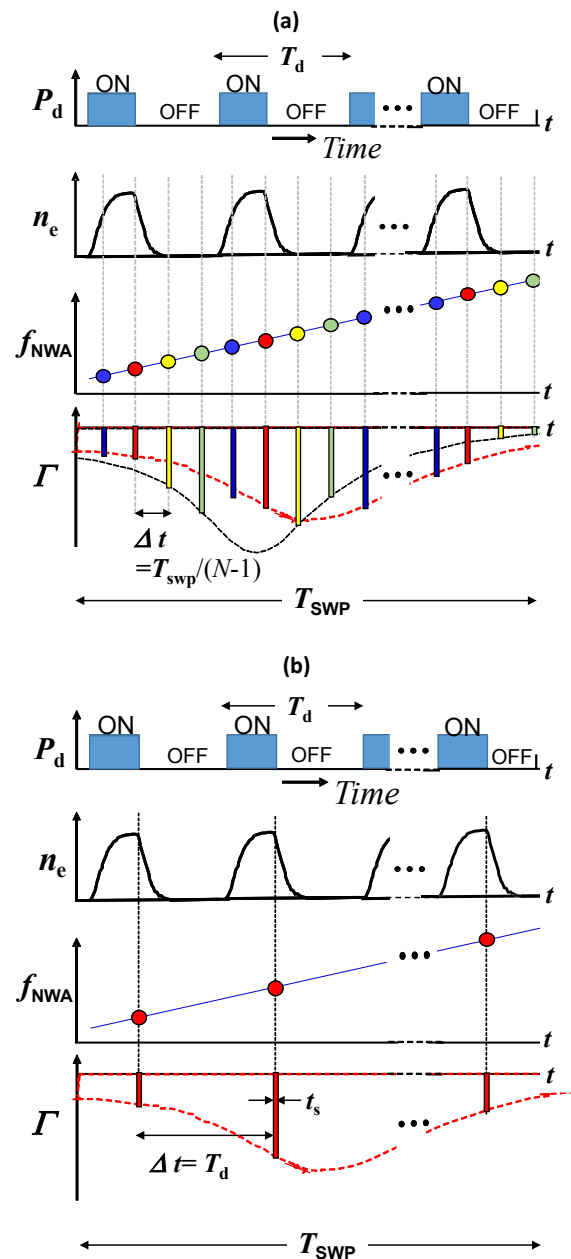


Fig. 2. (Color online) Schematic illustration of data acquisition by NWA in (a) the *on-sweep* mode and (b) the *on-point* mode. Temporal variations of discharge power, electron density, and reflectance.

of the reflectance Γ (S_{11} parameter) at a constant *phase* (*electron density*) of the modulated electron density, two data sampling modes of the NWA were used: the *on-sweep* mode and the *on-point* mode. In Fig. 2, we show the reflectance spectra for these two modes. When the discharge power P_d was switched on and off, the electron density n_e repeatedly varied in time, as shown in Fig. 2. The NWA frequency f_{NWA} was digitally swept, triggered by the synchronous output of the high-voltage pulse generator with the discharge pulse period T_d . Let the total number of the data points be N , with the NWA frequency sweep period denoted by T_{SWP} . In the *on-sweep* mode, a single discharge yields N data points at the frequency f_{NWA} , and the resultant reflectance Γ during the sweep period T_{SWP} is shown in Fig. 2(a). Thus, the m -th datum per single cycle of the discharge pulse is given by

$$(N - 1) \frac{T_d}{T_{SWP}} = m. \quad (2)$$

When m is not integer, different reflectance spectra are observed for different sweeps, as reported previously.²⁹⁾ To obtain a stable reflection spectrum, the parameters N , T_d , and T_{SWP} should be adjusted to obtain integer m . This is the so-called *synchronization* condition²⁹⁾ associated with *on-sweep* mode measurements. The reflectance spectrum that is obtained under the above condition is complex, owing to the mixing of Γ with different phases (electron densities). A well-defined data analysis algorithm is required for extracting a time-resolved reflectance spectrum from a mixture of frequency spectra. An example of such data analysis will be described in Sect. 4.

3.2 On-point mode

In the *on-point* mode, each discharge trigger drives a single frequency f_{NWA} (one datum) per discharge pulse, and the reflectance is measured at the constant *phase* (constant *electron density*) of the discharge pulse, as shown in Fig. 2(b). In other words, the discharge pulse period T_d is equal to the data sampling period $\Delta t = T_{SWP}/(N - 1)$, and substituting this relation into Eq. (2) leads to $m = 1$. Thus, the *on-point* mode automatically satisfies the synchronization condition. A single frequency sweep of the NWA yields n different frequency values at the same electron density [the middle panel of Fig. 2(b)]. As a result, the reflectance spectrum at the observing *phase* (*electron density*) is immediately obtained [the bottom panel of Fig. 2(b)] without the post-analysis of data that is required in the *on-sweep* mode. This is one of the advantages of using the *on-point* mode, while another advantage is the applicability of this method to higher pulse repetition frequencies, with better temporal resolution.

Because the *on-point* mode yields only one datum of electron density at the trigger time, the NWA triggering should be delayed during the discharge pulse period, for obtaining a full picture of temporal changes in the electron density. The time delay pitch Δt_D should be as small as possible for increasing the number of the measurement points during one pulse cycle. For example, with $\Delta t_D = 0.1 \mu s$ the data can be acquired every $0.1 \mu s$, making the *apparent* temporal resolution is $0.1 \mu s$. However, the *true* temporal resolution is determined by other factors, as discussed below.

3.3 Temporal resolution

NWA uses a super heterodyning detection system, i.e., the incoming signal is mixed with a local oscillator signal to obtain an intermediate frequency (IF), which is then passed through a band pass filter (IFBF). The IFBF acts as a window for detecting the signals; hence, the temporal resolution is approximately given by a reciprocal relation with the resonance bandwidth (RBW) of the IF filter. For instance, for the RBW of 100 kHz, the sampling time t_s per datum is $\sim 10 \mu s$. If the pulse discharge period T_d is shorter than the sampling time t_s , there will be instances in which IF measurements will yield no pulses, leading to poor trace noise. Therefore, measurements should be performed such that $t_s < T_d$.³⁰⁾ In the present study, we chose an RBW of 70 kHz in Agilent E5071C, which corresponds to $t_s \sim 14 \mu s$. On the other hand, the pulse discharge frequency was in the 0.5–25

kHz range, corresponding to the T_d in the 40–2000 μs range. Thus, all measurements were performed with the temporal resolution of $\sim 14 \mu s$, in the *on-point* mode.

4. Temporally resolved measurements in the on-sweep mode

Temporal variations in the electron density at the discharge pulse frequency below 0.5 kHz were measured for N_2 gas at 10 Pa, in the *on-sweep* mode. Figure 3(a) shows the reflectance spectra obtained for the 0.4 kHz discharge at 13% DR by fulfilling the synchronization condition in Eq. (2). The sweep time T_{SWP} was 2500 μs , and the number of data points were $N = 1601$ and $m = 10$. Therefore, the complex spectra correspond to 10 data points representing different pulse phases, at intervals of T_d/m (250 μs). The 1601 data points were divided into 10 groups ($m = 1-10$), such that the first group ($m = 1$) contained the data points with the indices of 1, 11, 21, ..., 1601, the second group ($m = 2$) contained the data points with the indices of 2, 12, 22, ..., 1592, and so on. The complex nature of the reflectance spectrum obtained in the *on-sweep* mode has already been discussed elsewhere.²⁹⁾

The ten groups form the reflectance Γ spectrum, and differ based on their phase, i.e., the time τ after the discharge turn-on. Three examples of time-resolved Γ spectra corresponding to the discharge times of $\tau = 250, 500, \text{ and } 750 \mu s$, are shown in Fig. 3(b). The resonance frequency obtained from these spectra was substituted into Eq. (1) for obtaining the electron density at the measured discharge time τ . Generally speaking, however, the CP exhibits two types of resonances; *volume wave* resonance and *surface wave* resonance.¹⁵⁾ Both frequencies f_0 and f in Eq. (1) denote the volume-wave resonance frequency f_{vwr} , while the n_e (cm^{-3}) is calculated from the surface-wave resonance frequency f_{swr} (GHz) as

$$n_e = \frac{1 + \epsilon_d}{0.806} f_{swr}^2 \times 10^{10}, \quad (3)$$

where the dielectric constant ϵ_d is 3.78 (quartz) for the present CP. In a high density case ($n_e > 10^{11} \text{ cm}^{-3}$), both resonances are simultaneously observed with the frequencies related through $f_{swr} < f_p < f_{vwr}$ for the electron plasma frequency f_p .¹⁵⁾ In low density plasma, however, only the volume-wave resonance appears as the spectrum measured at the specified discharge time in Fig. 3(b). In fact, the use of Eq. (1) in the present experiment yields low electron density ($n_e < 3 \times 10^9 \text{ cm}^{-3}$) in Fig. 3(c). A cross-check was performed in a DC glow discharge at the nitrogen pressure of 40 Pa, for comparing the results with Langmuir probe measurement. The electron density measured by using the CP was $1.87 \times 10^9 \text{ cm}^{-3}$ while the value determined by using the Langmuir probe was $1.45 \times 10^9 \text{ cm}^{-3}$. These values are quite close, indicating a good agreement between the CP and Langmuir probe-based measurements.

By sufficiently delaying the trigger time, we obtained temporally resolved reflectance (S_{11}) at various times τ after the discharge ignition. The volume-wave resonance frequencies thus obtained can be used for measuring the temporal evolution of the electron density, as shown in Fig. 3(c).

Experiments were also performed at a pulsed frequency higher than 0.5 kHz. However, the measured reflectance spectrum was irregular, and the time-resolved electron density was scattered, suggesting some measurement errors.

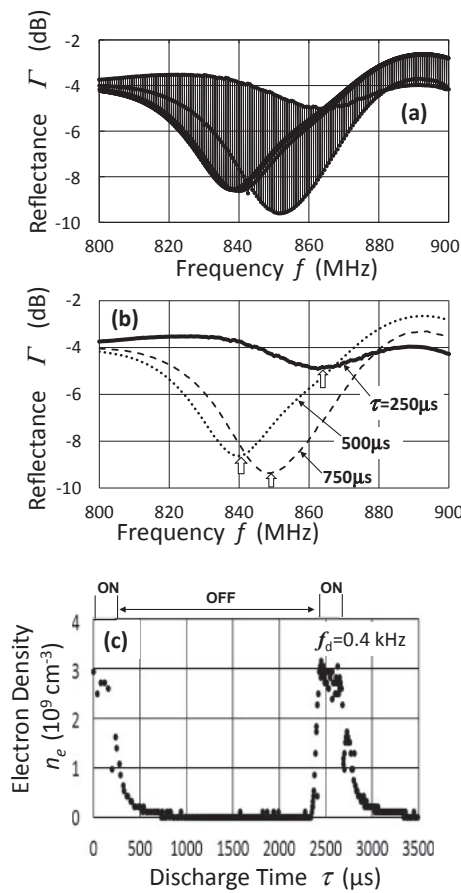


Fig. 3. (a) Reflectance spectra obtained in the *on-sweep* mode for the 0.4 kHz discharge with 13% DR at 10 Pa nitrogen. (b) Reflectance spectra for the discharge times of $\tau = 250, 500,$ and $750 \mu\text{s}$, for the data in (a). (c) Electron density as a function of the discharge time, for the data in (a).

This scattering increased with increasing the pulse frequency and duty cycle ratio. With low-frequency pulses, the NWA sweeps the frequency in the full span per the received trigger. However, as the pulse frequency increases, the NWA cannot make a full span sweep but requires intermission among the divided ranges of the frequency sweep, yielding timing errors for data acquisition in the *on-sweep* mode. In such high-frequency pulsed discharge, the *on-point* mode is available, as described below.

5. Temporally resolved measurements in the *on-point* mode

Temporal variations in the electron density were measured in the *on-point* mode of NWA E5071C, at the discharge pulse frequency above 1 kHz. Figure 4 shows example results for a 1 kHz discharge with 30% DR, for which the discharge voltage and current are shown in Figs. 4(b) and 4(c), respectively. Note that the glow discharge was conducted in the abnormal glow regime. Three sample reflectance spectra, for discharge times $\tau = 0, 10,$ and $20 \mu\text{s}$, obtained in the *on-point* mode, are shown in Fig. 4(a). Here, the arrow for each spectrum indicates the location of the resonance frequency, which in turn yields the electron density, as shown in Fig. 4(c).

The DR was increased to observe the temporal dependence of the electron density for the 1 kHz discharge. Figure 5 shows the results measured in the *on-point* mode, for the DR values of 10, 20, 40, and 50%. The electron density increases

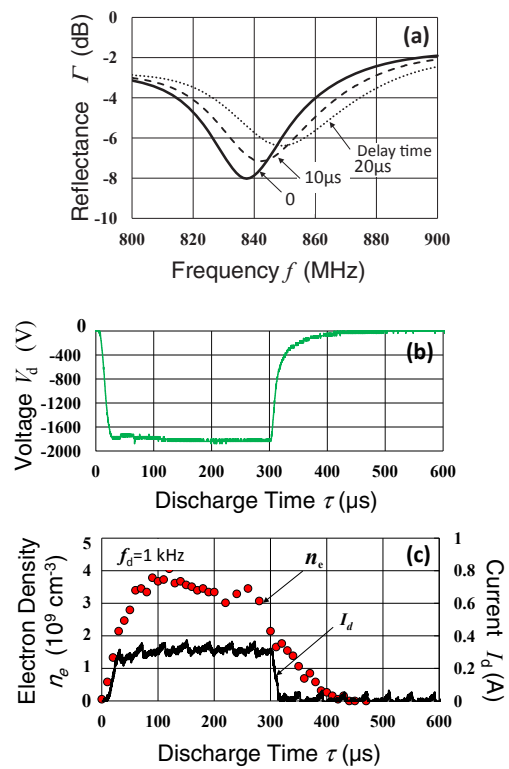


Fig. 4. (Color online) (a) Reflectance spectra measured at different delay times in the *on-point* mode. (b) Discharge voltage as a function of the discharge time. (c) Temporal evolution of electron density and discharge current for the 1 kHz discharge with 30% DR at 10 Pa nitrogen.

and then saturates, following the discharge current trend until $\tau = T_{\text{ON}}$. After the discharge is terminated ($\tau > T_{\text{ON}}$), the current rapidly decreases to zero, but the electron density decreases much slower, on the time scale of $100 \mu\text{s}$, in the afterglow regime. The maximal density in the active glow regime decreases with increasing the DR as the peak discharge current decreases with increasing the T_{ON} .

The *on-point* technique was successfully extended to discharge pulse frequencies of up to 5 kHz with 50% DR. The minimal trigger delay time in the presently used NWA E5071C was $10 \mu\text{s}$. For instance, at the pulse frequency of 10 kHz with 20% DR, the discharge on time T_{ON} was only $20 \mu\text{s}$, allowing the acquisition of only two data points for $\tau < T_{\text{ON}}$. To overcome this data deficit, an external signal delay device (Hewlett-Packard 8116A) was used for delaying the trigger signal, which enabled delaying the trigger signal to a minimum of $2 \mu\text{s}$. It should be noted here that the data was acquired every $2 \mu\text{s}$; however, it does not mean that the temporal resolution was $2 \mu\text{s}$. As described in Sect. 3.3, the temporal resolution was $\sim 14 \mu\text{s}$, as determined by the RBW of NWA. Thus, the measured electron density was regarded as the value averaged over the time window of $\sim 14 \mu\text{s}$.

This method was applied to a pulse discharge frequency of 10 kHz with 50% DR. The synchronous output from the high-voltage pulse generator was delayed by $2 \mu\text{s}$ before it was fed into the NWA. Figure 6 shows the temporal changes in the electron density along with the discharge voltage for the 10 kHz pulse. It should be noted here that the electron density at $\tau = 0$ was not zero and the plasma continued over the discharge on and off. Namely, the plasma slowly decayed and survived during the afterglow. Such plasma continuation was

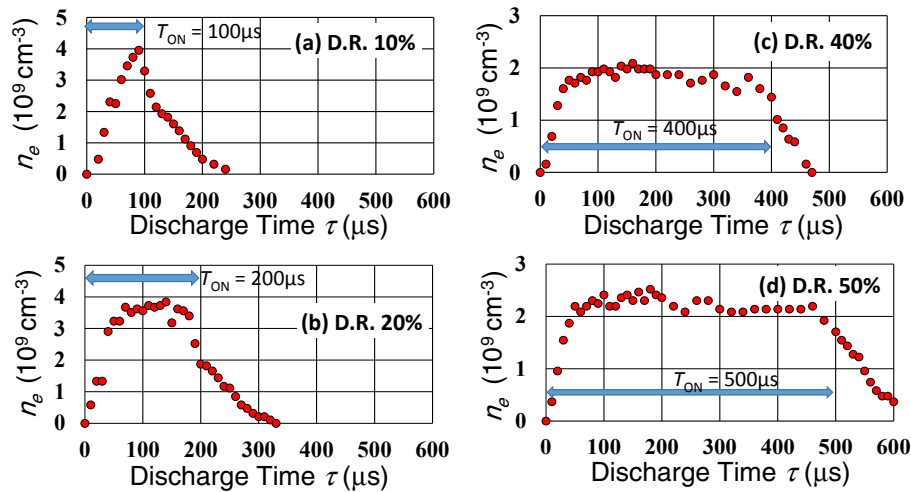


Fig. 5. (Color online) Time-resolved measurement of electron density for the 1 kHz discharge at 10 Pa nitrogen with duty cycle ratio of (a) 10, (b) 20, (c) 40, and (d) 50%.

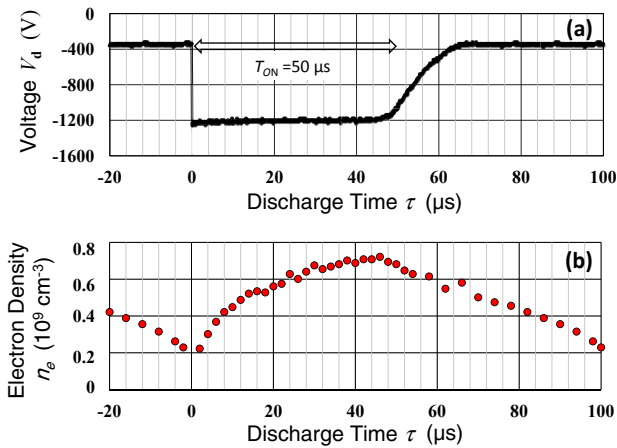


Fig. 6. (Color online) (a) Temporal variation of the discharge voltage for the 10 kHz discharge with 50% DR at 10 Pa nitrogen, together with (b) the electron density measured in the *on-point* mode.

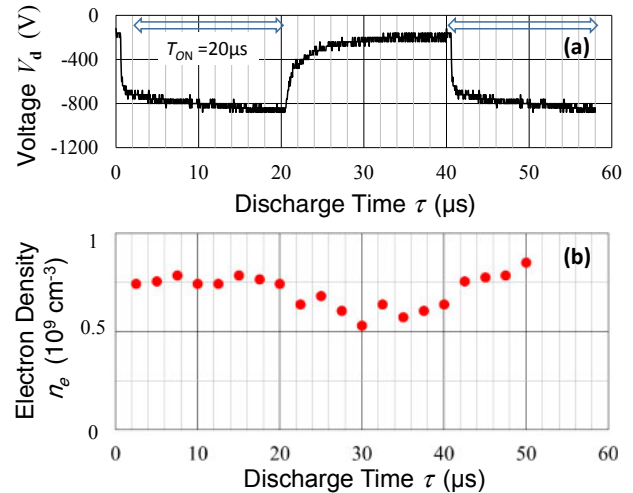


Fig. 7. (Color online) (a) Temporal variation of the discharge voltage for the 25 kHz discharge with 50% DR at 10 Pa nitrogen, together with (b) the electron density measured in the *on-point* mode.

more clearly observed at the pulse frequency of 25 kHz at 50% DR, as shown in Fig. 7.

6. Electron density decay in the afterglow region

To investigate the nature of the electron density decay in the afterglow, nitrogen and argon discharge characteristics were compared for the same pulse frequency of 1 kHz with 30% DR at the pressure of 40 Pa. A reduction in the electron density in the afterglow region was measured as shown in Figs. 8(a) and 8(b) for the nitrogen and argon discharges, respectively. In the case of the nitrogen discharge, an exponential density reduction was observed [Fig. 8(a)], which could be simply expressed as $\exp(-t/\tau_D)$ with the time constant $\tau_D \sim 60 \mu\text{s}$. On the other hand, the argon afterglow data [Fig. 8(b)] exhibited a three-step decay: $\tau_D \sim 50 \mu\text{s}$ during step (i), $\tau_D \sim 400 \mu\text{s}$ during step (ii), and $\tau_D \sim 100 \mu\text{s}$ during step (iii).

To understand the difference between the afterglow density decay behaviors of the nitrogen and argon discharges, we performed Langmuir probe measurements in a simplified condition of DC discharge, at the pressure of 40 Pa, where the discharge voltage and current were $V_d = -700 \text{ V}$ and $I_d = 150 \text{ mA}$ for the nitrogen discharge, and $V_d = -600 \text{ V}$ and

$I_d = 150 \text{ mA}$ for the argon discharge. Figure 9 shows semi-logarithmic plots of the measured probe currents, as a function of the probe voltage. The slope of the straight line fitted to the measured points yielded the electron temperature $T_e \sim 0.3 \text{ eV}$ for the nitrogen discharge, while the argon plasma exhibited a bi-Maxwellian type of electron energy distribution function, with bulk temperature $T_{\text{eb}} \sim 0.9 \text{ eV}$ and hot tail temperature $T_{\text{eh}} \sim 2 \text{ eV}$. Thus, the argon plasma has abundant high-energy electrons, which are attributed to the secondary electrons that are emitted from the cathode. In the afterglow, the high-energy electrons are immediately lost during step (i), because they can escape through a potential barrier around the cathode and anode. As the time goes on, the bulk electron temperature gradually decreases during step (ii). When the temperature drops to $\sim 0.2 \text{ eV}$, the rate of electron-neutral collisions decreases, owing to Ramsauer effect.³¹⁾ Thus, the electron diffusion loss is enhanced, leading to a smaller value of τ_D during step (iii).

On the other hand, because N_2 is a molecular gas, the high-energy electrons in plasma are easily lost through many loss channels of inelastic collisions that excite the gas to

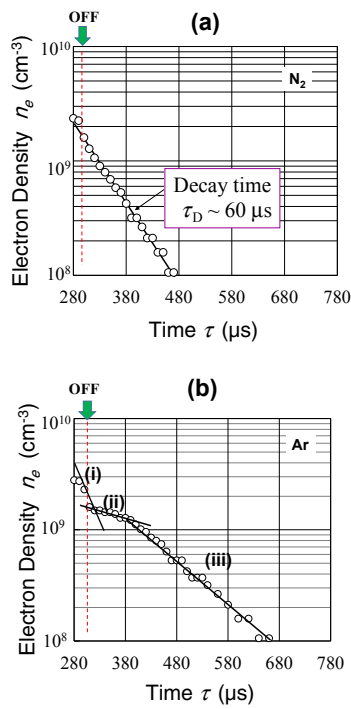


Fig. 8. (Color online) Electron density decay in afterglow for the 1 kHz discharge at 40 Pa in (a) nitrogen and (b) argon.

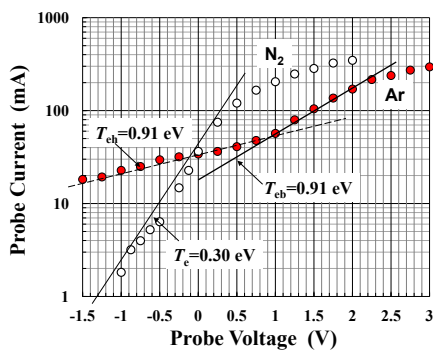


Fig. 9. (Color online) Semi-logarithmic plot of the probe electron current and the probe voltage for the DC discharges at 40 Pa in nitrogen and argon.

vibrational and rotational energy levels, along with dissociation processes.³² This explains why only a very weak high-energy tail was observed in the nitrogen DC discharge [Fig. 8(a)]. In the afterglow region of a pulsed discharge, a monotonic exponential decay of the electron density was observed, probably owing to a weak Ramsauer effect in the case of nitrogen.

7. Conclusions

Curling probe (CP) technique was applied to time-resolved measurements of electron density in pulsed DC glow plasmas. Because the CP resonance frequency is time-dependent, the NWA yielded complex reflectance spectra when operated in the *on-sweep* mode. The complex spectra obtained in the *on-sweep* mode were applicable for time-resolved electron density measurements at low pulse frequencies (below 0.5 kHz). For higher pulse discharge frequencies (up to 25 kHz), the *on-point* NWA mode was introduced, wherein each discharge trigger yielded one datum of reflectance at a single frequency. A proper delay of the discharge trigger

provided a minimal time interval of 2 μs in the time-resolved measurements. The decay time constant of electron density in afterglow was investigated for a discharge in nitrogen and was compared with that for a pulsed discharge in argon. A three-step decay was observed in the case of argon. This phenomenon was tentatively attributed to a bi-Maxwellian type of electron energy distribution and to Ramsauer effect with Langmuir probe data taken into account.

In conclusion, we demonstrated that curling probes can be used for time-resolved measurements of electron density in plasma processing. The temporal resolution is limited by the NWA that is used: modern pulse NWAs, such as Keysight PNA series, can provide temporal resolution of ~20 ns.

- 1) F. F. Chen, in *Plasma Diagnostic Techniques*, ed. R. H. Huddleston and S. L. Leonard (Academic Press, New York, 1965) p. 113.
- 2) T. Shirakawa and H. Sugai, *Jpn. J. Appl. Phys.* **32**, 5129 (1993).
- 3) H. Kokura, K. Nakamura, I. P. Ganashev, and H. Sugai, *Jpn. J. Appl. Phys.* **38**, 5262 (1999).
- 4) K. Nakamura, M. Ohata, and H. Sugai, *J. Vac. Sci. Technol. A* **21**, 325 (2003).
- 5) M. Lapke, T. Mussenbrock, R. P. Brinkmann, C. Scharwitz, M. Boeke, and J. Winter, *Appl. Phys. Lett.* **90**, 121502 (2007).
- 6) H. Sugai, I. Ganashev, M. Hosokawa, K. Mizuno, and K. Nakamura, *Plasma Sources Sci. Technol.* **10**, 378 (2001).
- 7) O. Hirano, K. Nakamura, and H. Sugai, Proc. 6th Int. Conf. Reactive Plasmas/23rd Symp. Plasma Processing, 2006, p. 727.
- 8) K. Kinoshita, K. Nakamura, O. Hirano, Y. Hyodo, O. Kiso, J. Kawahara, Y. Hayashi, S. Saito, H. Sugai, and T. Kikkawa, 56th Int. Symp. Exhib. Abstr. American Vacuum Society, 2006, p. 149.
- 9) K. Nakamura, H. Sugai, N. Noda, J. Kawahara, O. Kiso, and K. Kinoshita, Proc. Int. Symp. Dry Process, 2004, p. 169.
- 10) S. Dine, J. P. Booth, G. A. Curley, C. S. Corr, J. Jolly, and J. Guillon, *Plasma Sources Sci. Technol.* **14**, 777 (2005).
- 11) M. Lapke, T. Mussenbrock, and R. P. Brinkmann, *Appl. Phys. Lett.* **93**, 051502 (2008).
- 12) C. Scharwitz, M. Böke, J. Winter, M. Lapke, T. Mussenbrock, and R. P. Brinkmann, *Appl. Phys. Lett.* **94**, 011502 (2009).
- 13) R. L. Stenzel, *Rev. Sci. Instrum.* **47**, 603 (1976).
- 14) R. B. Piejak, V. A. Godyak, R. Garner, and B. M. Alexandrovich, *J. Appl. Phys.* **95**, 3785 (2004).
- 15) I. Liang, K. Nakamura, and H. Sugai, *Appl. Phys. Express* **4**, 066101 (2011).
- 16) A. Pandey, S. Ikezawa, K. Nakamura, and H. Sugai, Abstr. 65th Gaseous Electronics Conf., 2012, p. 23.
- 17) K. Yee, *IEEE Trans. Antennas Propag.* **14**, 302 (1966).
- 18) Web [<http://www.aceknack.com/>].
- 19) A. Pandey, H. Imai, D. Kanematsu, S. Ikezawa, K. Nakamura, and H. Sugai, Proc. 34th Int. Symp. Dry Process, 2012, p. 45.
- 20) A. Pandey, K. Nakamura, and H. Sugai, *Appl. Phys. Express* **6**, 056202 (2013).
- 21) R. W. Boswell and R. K. Porteous, *J. Appl. Phys.* **62**, 3123 (1987).
- 22) P. Jiang, D. J. Economou, and C. B. Shin, *Plasma Chem. Plasma Process.* **15**, 383 (1995).
- 23) J. Verdeyen, J. Beberman, and L. Overzet, *J. Vac. Sci. Technol. A* **8**, 1851 (1990).
- 24) A. Bouchoule and P. Ranson, *J. Vac. Sci. Technol. A* **9**, 317 (1991).
- 25) A. Bouchoule, A. Plain, L. Boufendi, J. Ph. Blondeau, and C. Laure, *J. Appl. Phys.* **70**, 1991 (1991).
- 26) Y. Watanabe, M. Shiratani, and H. Makino, *Appl. Phys. Lett.* **57**, 1616 (1990).
- 27) S. K. Park and D. J. Economou, *J. Electrochem. Soc.* **138**, 1499 (1991).
- 28) P. Subramonium and M. J. Kushner, *J. Appl. Phys.* **96**, 82 (2004).
- 29) A. Pandey, W. Sakakibara, H. Matsuoka, K. Nakamura, and H. Sugai, *Appl. Phys. Lett.* **104**, 024111 (2014).
- 30) J. P. Dunsmore, *Handbook of Microwave Component Measurement with Advanced VNA Technique* (Wiley, New York, 2012) 1st ed., p. 365.
- 31) S. C. Brown, *Introduction to Electrical Discharges* (Wiley, New York, 1966) 1st ed., p. 6.
- 32) M. A. Lieberman and A. J. Lichtenberg, *Principles of Plasma Discharges and Materials Processing* (Wiley, New York, 2005) 2nd ed., p. 82.